XIII International Conference on Computational Plasticity. Fundamentals and Applications
COMPLAS XIII
E. Oñate, D.R.J. Owen, D. Peric & M. Chiumenti (Eds)

LOWER BOUND ELEMENT AND SUBMODEL FOR MODELLING OF JOINTS BETWEEN PRECAST CONCRETE PANELS

MORTEN A. HERFELT*, PETER N. POULSEN†, LINH C. HOANG†, AND JESPER F. JENSEN*

*ALECTIA A/S
Teknikerbyen 34, 2830 Virum, Denmark
e-mail: mahe@alectia.com, http://www.alectia.com/

†Department of Civil Engineering
Technical University of Denmark
Brovej, Building 118, 2800 Kgs. Lyngby, Denmark
e-mail: pnp@byg.dtu.dk, http://www.byg.dtu.dk

Key words: Finite Element, In-situ Cast Joins, Limit Analysis, Precast Concrete Panels, Rigid Plasticity, Yield Criterion

Abstract. In practice, precast concrete structures are designed using either analytical methods or linear finite element tools, and the in-situ cast joints between the precast panels are assessed using conservative empirical design formulas. This often leads to a suboptimal design, and local mechanisms inside the joint are not taken into account. This paper presents an equilibrium element representing in-situ cast joints and an advanced submodel yield criterion is developed. The element and submodel are verified by comparison to a detailed numerical model as well as experimental results. The computational time and problem size of the joint element and detailed model will be discussed.

1 INTRODUCTION

Modern precast concrete element buildings use disk systems, i.e. precast wall panels and in-situ cast joints, to transfer horizontal and vertical forces from the facades and decks to the foundations of the building. The forces are transferred as in-plane forces, and the shear capacity of the walls and especially the joints are of the utmost importance. The shear capacity of such walls are in practice assessed by analytical models, i.e. yield lines or strut-and-tie models, or linear finite element analysis. This practice leads to suboptimal designs.

The in-situ cast joints between the precast panels are of particular interest. They are often the weakest part of the structure and they have some special mechanical properties.

The joints consist of a concrete core and two interfaces. The core is often reinforced in two directions, and the interfaces are often keyed. The shear capacity of the joints and interfaces are assessed by simple empirical design formulas [1], which often give a conservative estimate of the capacity.

Several researchers have investigated the behaviour of in-situ cast joints and interfaces. The investigations cover both experimental testing [2, 3, 4] and rigid plastic models, e.g. yield line analysis, [5, 6]. The analytical methods have been able to capture the behaviour observed in the experiments to a certain extent. Investigations using numerical tools, e.g. finite element methods, have primarily been focused on single key joints used in precast segmental bridges [7, 8]. These investigations have primarily been carried out by use of non-linear finite element analysis, which is heavy computationally, especially when considering that the ultimate load capacity is the result of main interest.

Numerical limit analysis is an alternative to the standard finite element formulation. The method is based on the extreemum principles for rigid-plastic materials [see e.g. 6, 9, 10] and a discretisation known from the finite element method. Anderheggen and Knöpfel [11] presented a general formulation and equilibrium elements for plates and solids. Several authors have contributed and equilibrium elements for stringers, bars, beams, disks, shells, and solids have been formulated [12, 13, 14, 15]. Most yield conditions relevant for structural engineering can be formulated as either second-order constraints or semi-definite constraints (linear matrix inequalities).

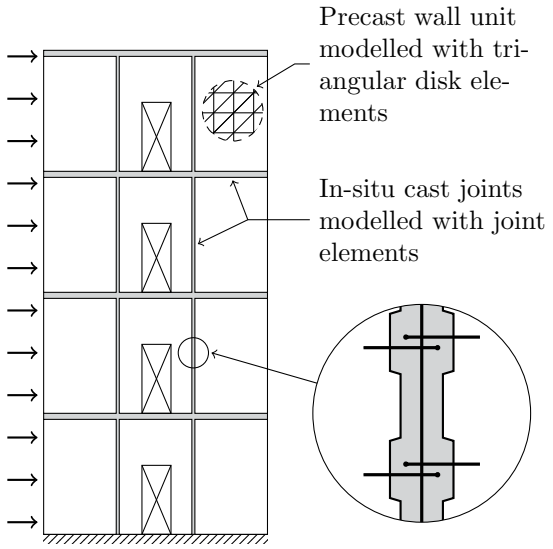

Figure 1: Four storey wall subjected to horizontal forces: The wall consists of 12 precast panels and joints. An example of a mesh (discretisation) for numerical analysis is seen for the top right panel.

Herfelt et al. [16] presented a detailed numerical rigid plastic model of keyed joints. The model used a lower bound formulation and the analysis determined a statically admissible stress field as well as the failure mode from the dual problem (i.e. corresponding upper

bound problem). The detailed model [16] used tringular disk elements [13, 14] representing the concrete, bar elements representing the reinforcement [13], and interface elements representing the interfaces between the precast and in-situ cast concrete.

The detailed numerical model predicts the shear capacity and failure mode of keyed joints reasonably well, however, the model is not feasible for practical modelling of larger panel structures due to the size of the model and computational time required. Fig. 1 shows a four storey wall consisting of several precast panels and in-situ cast joints. As indicated in the figure, a joint element is needed for practical modelling.

This paper presents an equilibrium element representing the in-situ cast joints. The element is designed for interaction with the disk element [13, 14] and interface elements [16], which both have a linear stress variation, and the scope is to be able to model entire disk systems, e.g. the wall seen in Fig. 1. An advanced submodel yield criterion based on the stringer method is developed. The scope of the submodel is to capture some of the keyed mechanisms identified by the detailed model [16]. The submodel will require second-order conic constraints and will fit the format of second-order cone programming (SOCP). The joint element and submodel yield criterion will be compared to the detailed numerical model [16] as well as experimental results [2].

2 PROBLEM FORMULATION

Numerical limit analysis is formulated as an optimisation problem, where the goal is to maximise a load factor λ. The analysis determines a statically admissible stress field, i.e. a stress field that satisfies equilibrium and does not violate the yield criteria in any point.

$$\begin{aligned} &\text{maximise} && \lambda \\ &\text{subject to} && \boldsymbol{H}\,\boldsymbol{\beta} = \lambda\,\boldsymbol{R} + \boldsymbol{R}_0 \\ &&& f(\boldsymbol{\beta}_i) \leq 0, \qquad i = 1, 2, \ldots, m \end{aligned} \tag{1}$$

The linear equality constraints ensure equilibrium, while the functions $f\left(\boldsymbol{\beta}_i\right) \leq 0$ ensure that the stress field does not violate the yield criteria. The load consists of a constant part $\boldsymbol{R}_0$ and a scalable part $\boldsymbol{R}\,\lambda$. $\boldsymbol{H}$ is the equilibrium matrix, and β is the stress vector.

The yield function f is generally convex, but non-linear, thus, the optimisation problem will be a convex problem. The type of problem depends on the chosen yield function, and the work presented in this paper will be formulated for second-order cone programming, a subclass of convex programming [17].

3 KEYED JOINTS

A keyed joint reinforced with U-bars and a locking bar is considered. Fig. 2 shows the basic design of a keyed joint: The vertical solid lines represent U-bars, and the horizontal solid line represents the locking bar. The local coordinate system (n, t) is also seen in Fig. 2. A unit section of the joint is indicated with a dashed rectangle; this (repeatable) unit section will be the basis of an advanced submodel yield criterion for the equilibrium joint

element. The width of the joint, b, is usually narrower than 100 mm and the thickness t below 250 mm. The length of the joint, on the other hand, ranges from a single storey height to the height of the entire building.

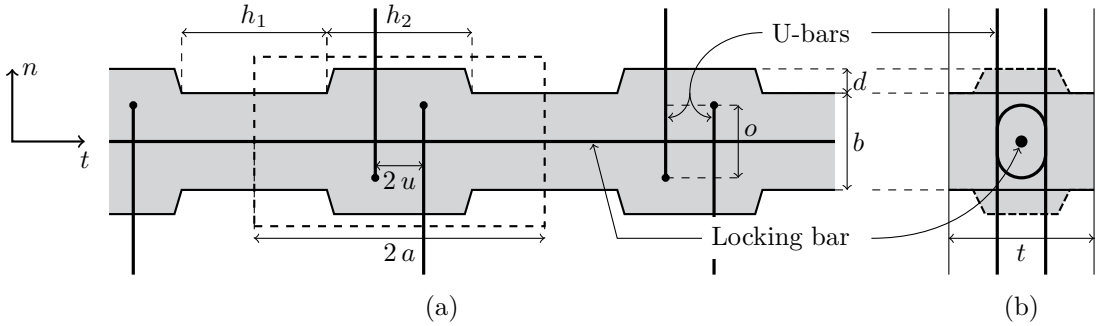

Figure 2: The basic design of a keyed joint reinforced with U-bars: a) elevation, b) cross section.

4 JOINT ELEMENT

An equilibrium element representing in-situ cast joints is needed for practical modelling of precast concrete panel structures. The joint element will dictate the distribution and transfer of stresses through the joint. The element is designed to be compatible with the linear stress triangle (disk element) [13, 14], thus, the joint element must have a linear variation of the shear stress and transverse normal stress, and a quadratic variation of the longitudinal normal stress

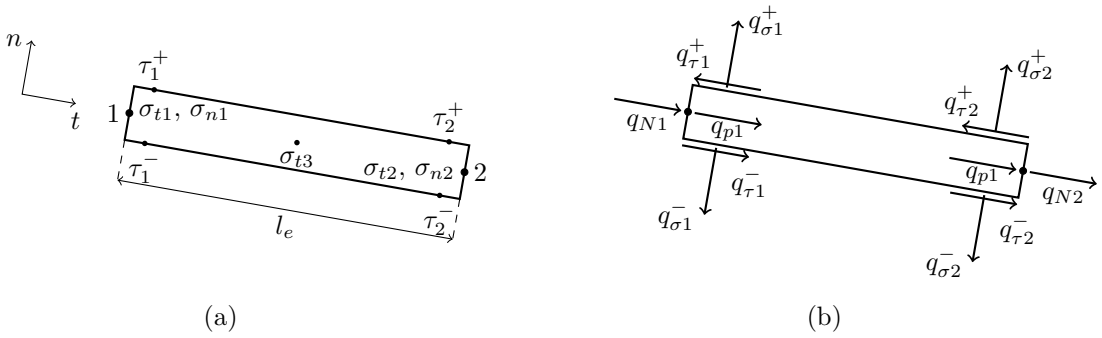

Figure 3: Joint element: a) Geometry, stress variables, and local coordinate system. b) Nodal forces for the equilibrium equations.

Fig. 3 shows the equilibrium element. The length and orientation of the element are defined by the two nodes seen in Fig. 3(a) (indicated by 1 and 2). The element has 9 stress variables seen in Fig. 3(a). The equilibrium equations of the element can be written as follows

$$\boldsymbol{q}_{el} = \boldsymbol{h}_{el}\,\boldsymbol{\beta}_{el} \tag{2}$$

where $\boldsymbol{\beta}_{el}$ is a vector containing the 9 stress variables, $\boldsymbol{q}_{el}$ contains the 12 nodal forces seen in Fig. 3(b), and $\boldsymbol{h}_{el}$ is the element equilibrium matrix (for this element a 12×9 matrix). The equilibrium matrix $\boldsymbol{h}_{el}$ and the stress vector $\boldsymbol{\beta}_{el}$ are explicitly given in (3).

$$\boldsymbol{q}_{el} = \begin{bmatrix} q^+_{\sigma 1} \\ q^+_{\tau 1} \\ q^+_{\sigma 2} \\ q^+_{\tau 2} \\ \hdashline q^-_{\sigma 1} \\ q^-_{\tau 1} \\ q^-_{\sigma 2} \\ q^-_{\tau 2} \\ \hdashline q_{N1} \\ q_{N2} \\ q_{p1} \\ q_{p2} \end{bmatrix} = \left[\begin{array}{ccccccccc} t & 0 & 0 & 0 & 0 & 0 & 0 & 0 & 0 \\ 0 & 0 & -t & 0 & 0 & 0 & 0 & 0 & 0 \\ 0 & t & 0 & 0 & 0 & 0 & 0 & 0 & 0 \\ 0 & 0 & 0 & -t & 0 & 0 & 0 & 0 & 0 \\ \hdashline -t & 0 & 0 & 0 & 0 & 0 & 0 & 0 & 0 \\ 0 & 0 & 0 & 0 & t & 0 & 0 & 0 & 0 \\ 0 & -t & 0 & 0 & 0 & 0 & 0 & 0 & 0 \\ 0 & 0 & 0 & 0 & 0 & t & 0 & 0 & 0 \\ \hdashline 0 & 0 & 0 & 0 & 0 & 0 & bt & 0 & 0 \\ 0 & 0 & 0 & 0 & 0 & 0 & 0 & -bt & 0 \\ 0 & 0 & t & 0 & -t & 0 & 3\frac{bt}{l_e} & \frac{bt}{l_e} & -4\frac{bt}{l_e} \\ 0 & 0 & 0 & t & 0 & -t & -\frac{bt}{l_e} & -3\frac{bt}{l_e} & 4\frac{bt}{l_e} \end{array}\right] \begin{bmatrix} \sigma_{n1} \\ \sigma_{n2} \\ \tau^+_1 \\ \tau^+_2 \\ \tau^-_1 \\ \tau^-_2 \\ \sigma_{t1} \\ \sigma_{t2} \\ \sigma_{t3} \end{bmatrix} \tag{3}$$

The equilibrium matrix and generalised nodal force vector can be split into three parts; one for the positive side of the joint, one for the negative side of the joint, and one for the nodal forces in the longitudinal direction. It is assumed that the transverse normal stress (n-direction) is transferred directly through the joint, but this is not necessarily the case for the shear stresses, which may be used to built up an axial force in the longitudinal direction.

Each point along the joint element has a stress state defined by four stress parameters, σ_n, σ_t, τ^+, and τ^-. The yield criterion takes these four stress parameters as input. Five yield criterion check points evenly distributed along the length of the element are chosen for the joint element due to the quadratic varying normal stress in the t-direction.

5 SUBMODEL YIELD CRITERION

The submodel yield condition, i.e. the yield function for the joint element, is in itself a small optimisation problem, and the equilibrium model for the submodel is based on a stringer model [6, 12]. This study uses a modified stringer method where the panels have three stress components; confinement pressure is added instead of smeared reinforcement due to the scale of the model. This approach also allows for the optimisation to determine the optimal distribution of the confinement pressure.

This section describes the submodel that is used to determine the yield criterion for the joint element. The scope of the submodel is to capture some important local stress states within the joint as a result of different reinforcement layouts. Three modified stringer models are introduced for this purpose. The submodel is based on a unit section of the keyed joint (see Fig. 2). Fig. 4 shows the overall principle behind the submodel yield

criterion: Three statically admissible modified stringer models are combined using the superposition principle.

5.1 Assumptions for the submodel

It is assumed that the behaviour of the joint can be represented by three modified stringer models. The superposition principle is used to combine the three models, and the combined model is checked against the appropriate yield criteria to ensure a safe solution.

We assume a two dimensional stress state in the joint. This assumption may not be accurate near the U-bars due to their geometry, which necessarily will lead to a three-dimensional stress state in the joint. The modified stringer models only describe a two-dimensional stress state and out-of-plane mechanisms are neglected. This will lead to a lower shear capacity, and the submodel may underestimate the capacity in some cases.

5.2 Equilibrium equations of the submodel

It is necessary to mobilise the two U-bars in order to transfer tension or to establish confinement pressure on the joint. The stringer model for transfer transverse tension (see Fig. 4) gives the following relations:

$$\tau_{21} = \frac{V}{o\,t} = \frac{u}{a}\,\frac{T}{o\,t}, \qquad \tau_{22} = \left(\frac{u}{a} - 1\right)\,\frac{T}{o\,t} \tag{4}$$

From the antisymmetric stringer model it can be concluded that $\tau_{21} = \tau_{23}$. The stringer force V will usually be balanced out by an adjacent joint section.

The two horizontal boundaries may be subjected to shear stresses of different magnitudes, hence, the central stringer seen in Fig. 4 will carry a linear varying normal force. From Fig. 4 it follows that the shear stresses acting on the unit joint section are transferred directly to panels 1 and 3, respectively:

$$\tau^{+} = \tau_1, \qquad \tau^{-} = \tau_3 \tag{5}$$

The two shear panels 1 and 3 overlap the three panels of the second stringer model seen in Fig. 4, and the resulting stresses can simply be determined by adding up the shear stresses (superposition).

The concrete shear panels need either reinforcement or confinement pressure in two directions to be able to carry shear stresses. The confinement pressure may originate from externally applied compressive loads or from stresses developed to create internal equilibrium with tensile stresses in the reinforcement. The external loads seen in Fig. 4 must be in equilibrium, thus, the difference in the normal force must be equal to the difference in the shear forces:

$$F_t^{+} - F_t^{-} = 2\,a\,t\,\tau^{+} - 2\,a\,t\,\tau^{-} \tag{6}$$

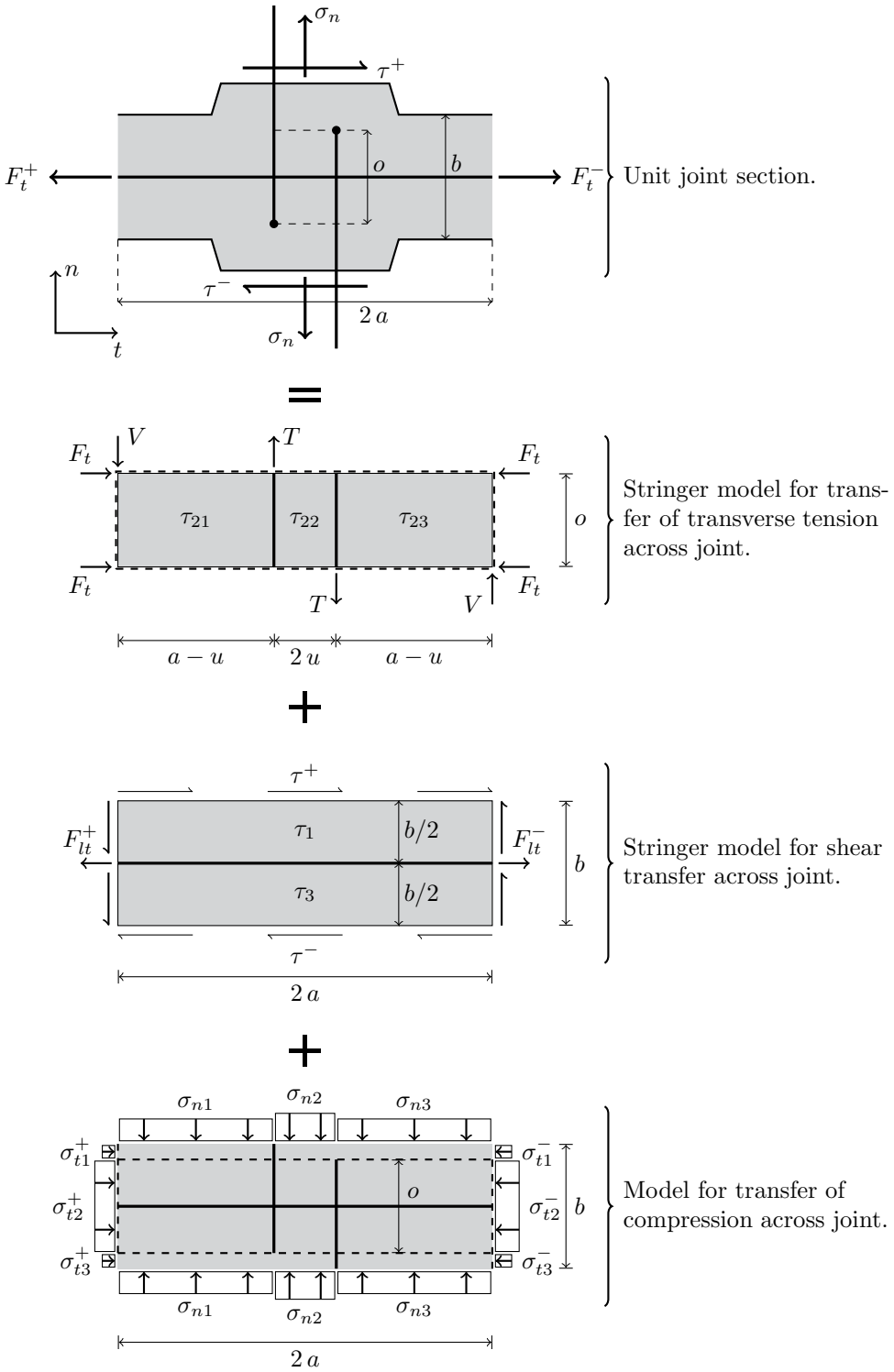

Figure 4: Unit joint section and the three stringer models. The behaviour of the unit joint section is divided into three main mechanisms, namely transverse tension, shear, and compression.

Vertical equilibrium at the horizontal boundaries gives:

$$2\,a\,t\,\sigma_n = T - V - (a-u)\,t\,(\sigma_{n1}+\sigma_{n3}) - 2\,u\,t\,\sigma_{n2} \tag{7}$$

and similarly for the horizontal forces:

$$\begin{aligned} F_t^+ &= F_{lt}^+ - 2\,F_t - \frac{b-o}{2}\,t\,(\sigma_{t1}^+ + \sigma_{t3}^+) - o\,t\,\sigma_{t2}^+ \\ F_t^- &= F_{lt}^- - 2\,F_t - \frac{b-o}{2}\,t\,(\sigma_{t1}^- + \sigma_{t3}^-) - o\,t\,\sigma_{t2}^- \end{aligned} \tag{8}$$

The necessary equilibrium equations of the submodel have now been established.

5.3 Yield conditions

The loop reinforcement and locking bar carry stringer forces. It is assumed that the reinforcement only carries tension, hence, the yield criterion can be stated as

$$0 \le T \le A_{su}\,f_{Yu}, \quad 0 \le F_{lt}^+ \le A_{sl}\,f_{Yl}, \quad \text{and} \quad 0 \le F_{lt}^- \le A_{sl}\,f_{Yl} \tag{9}$$

where A_{su} and A_{sl} are the cross section areas of the loop reinforcement and locking bar, respectively, and f_{Yu} and f_{Yl} are the uniaxial yield strength of the loop reinforcement and locking bar, respectively.

The concrete stringers (indicated by the thick dashed lines in Fig. 4) are treated differently as there are no reinforcement. Confinement pressure is necessary to ensure that the entire stringer is loaded in compression, which leads to the following linear inequality:

$$-F_t + \tau_{21}\,(a-u)\,t \le 0 \tag{10}$$

Each shear panel in the submodels has three stress components; the shear stress and two normal stresses. The modified Mohr-Coulomb yield criterion for plane stress is used as the yield criterion for the panels.

$$\begin{aligned} \sigma_1 &\le f_t \\ k\,\sigma_1 - \sigma_2 &\le f_c \\ -\sigma_2 &\le f_c \end{aligned} \tag{11}$$

where σ_1 and σ_2 are the largest and smallest principal stresses, respectively. f_t is the uniaxial tensile strength of the concrete, f_c is the effective uniaxial compressive strength, and k is a friction parameter. The yield condition is non-linear as it is given in terms of the principal stresses. By introducing three auxiliary variables, the yield condition can be formulated as a single conic constraint and three linear constraints [16].

6 ANALYSIS AND DISCUSSION

The joint element and submodel yield criterion are compared to the detailed numerical model [16] using the geometry and reinforcement layout of the tests by Hansen and Olesen [2]. The normalised shear capacity is plotted as a function of the mechanical reinforcement degree, respectively. The mechanical reinforcement degree is defined as

$$\Phi = \frac{\sum A_{su}\, f_{Yu}}{t\, l\, f_c} \tag{12}$$

where A_{su} is the cross section area of one U-bar, f_{Yu} is the yield strength of the U-bars, t is the thickness (see Fig. 2), and l is the total length of the joint.

The material parameters for the interface of the joint element, namely the cohesion and friction coefficient, are fitted to the curve for the detailed model. The size of the cohesion depends on both the geometry of the keys as well as the reinforcement layout. To simulate that the joint section is a part of a long joint the axial nodal forces q_{N1} and q_{N2} (see Eq. 3) are supported, hence, the force in the t-direction can be chosen freely by the optimiser.

Hansen and Olesen investigated the behaviour of keyed joints with different reinforcement layouts. Some of the experiments featured joints with a significant distance in-between the U-bars (see Fig. 5), which yielded a lower shear capacity and the concrete core was almost completely destroyed at failure.

The specimens had a length of 1200 mm, a width of 50 mm, and 14 keys total. The keys have a depth of $d = 6$ mm, a length of $h_2 = 40$ mm and the spacing between the keys is $h_1 = 40$ mm (see Fig. 2).

(a) Wall Joint: Specimen 24 (b) Wall Joint: Specimen 26

Figure 5: The two specimens with a significant distance between the U-bars tested by Hansen and Olesen [2], measurements in millimetres.

Fig. 5 shows the two specimen (24 and 26) which features a significant distance between the U-bars. For the remaining specimens the U-bars were placed with a distance of 10 mm. For specimens 24 and 26 the shear capacity is illustrated as a function of the reinforcement degree, and the results for all specimens is summed up in Tab. 1.

A friction coefficient of $\mu = 0.60$ is used for all interfaces. The compressive concrete strength of the joint concrete ranges from 13 MPa to 31 MPa (see Tab. 1), and the tensile strength of the concrete is taken as zero.

Fig. 6 shows that the joint element captures the same behaviour as the detailed model to a reasonable degree, and the plain interface combined with the *pseudo cohesion*

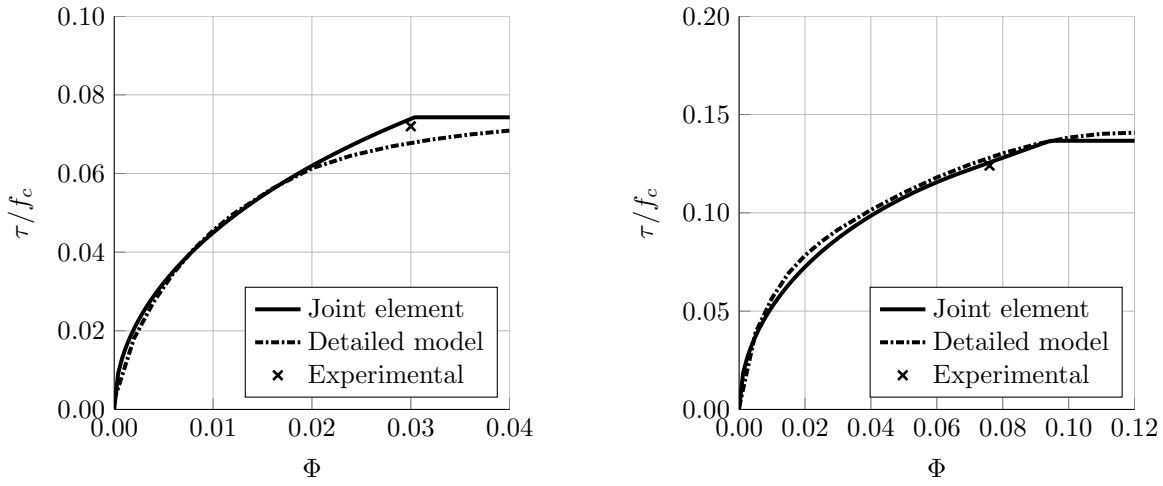

(a) Specimen 24

(b) Specimen 26

Figure 6: Comparison of a single joint element with a submodel yield criterion, a detailed model using several thousands elements, and experimental results for specimens 24 (a) and 26 (b).

represents the behaviour of the keyed interface well. The cohesion of the interface is taken as $c_{24} = 0.06\, f_c = 1.56$ MPa for specimen 24, and $c_{26} = 0.08\, f_c = 1.92$ MPa for specimen 26 for the best fit. The figure also who a decent correlation between the numerical results and the experiment.

Table 1: Results of the numerical models and experimental testing [2].

Specimen	f_c [MPa]	Φ -	τ/f_c **Experimental**	τ/f_c **Detailed model**	τ/f_c **Joint element**
23	31	0.025	0.080	0.083	0.075
24	26	0.030	0.072	0.068	0.074
25	24	0.076	0.161	0.131	0.126
26	24	0.076	0.124	0.128	0.126
27	15	0.139	0.213	0.189	0.193
28	13	0.235	0.286	0.230	0.242

Tab. 1 summarises the results of the joint element, the detailed numerical model, and the experimental testing. It is seen that the joint element gives a reasonable estimate of the shear capacity of keyed joints, and for practical design of structures, the joint element is superior as Tab. 2 shows. The detailed model is heavy computationally and the optimisation time also shows this, hence, the model is not feasible for lager precast structures. The analysis is performed on a desktop PC with 12 GB RAM memory and an

Intel Xeon processeor with 8 CPUs and 3.2 GHz. The analysis is performed in MatLab.

Table 2: Comparison of problem data for the joint element and detailed model [16].

	Joint element	Detailed model
Number of equilibrium elements	3	20,024
Number of variables	302	1,364,509
Number of linear constraints	388	1,305,890
Number of conic constraints	44	134,472
Optimisation time	0.43 s	97.89 s

7 CONCLUSION

An equilibrium joint element for lower bound limit analysis has been presented. The advanced submodel yield criterion makes the element capable of modelling in-situ cast keyed joints between precast concrete panels using a single element. The submodel yield criterion is based on three modified stringer models using the principle of superposition. The submodel makes it possible to take local effects in the joint into account. The joint element and submodel are formulated for second-order cone programming, which can be solved reliably and efficiently by interior point methods.

The single joint element and submodel are verified by comparison to a detailed numerical model, which uses several thousand equilibrium elements. The joint element and submodel are capable of capturing the critical mechanisms and predict the same behaviour as the detailed model. The computational time and problem size of the joint element makes it superior to the detailed model when it comes to practical design of precast concrete structures and modelling of real size structures.

REFERENCES

References

[1] European Committee for Standardization. En 1992-1-1 eurocode 2: Design of concrete structures - part 1-1: General rules and rules for buildings (2005).

[2] Hansen, K. and Olesen, S. O. *SBI-Report 97: Keyed Shear Joints* (Statens Byggeforskningsinstitut, 1976).

[3] Fauchart, J. and Cortini, P. Étude expérimentale de joints horizontaux entre panneaux préfabriqués pour murs de batiments. *Annales de L'Institut Technique du Batiment et dês Travaux Publics* **300**, 86–103 (1972).

[4] Joergensen, H. B. and Hoang, L. C. Tests and limit analysis of loop connections

between precast concrete elements loaded in tension. *Engineering Structures* **52**, 558–569 (2013).

[5] Jensen, B. C. On the ultimate load of vertical, keyed shear joints in large panel buildings. In *Symposium on Bearing Walls in Warsaw* (1975).

[6] Nielsen, M. P. and Hoang, L. C. *Limit Analysis and Concrete Plasticity, Third Edition* (Taylor and Francis, 2010).

[7] Issa, M. A. and Abdalla, H. A. Structural behavior of single key joints in precast concrete segmental bridges. *Journal of Bridge Engineering* **12**, 315–324 (2007).

[8] Kaneko, Y. and Mihashi, H. Analytical study on the cracking transition of concrete shear key. *Materials and Structures* **32**, 196–202 (1999).

[9] Hill, R. On the state of stress in a plastic-rigid body at the yield point. *The London, Edinburgh, and Dublin Philosophical Magazine and Journal of Science* **42**, 868–875 (1951).

[10] Drucker, D., Prager, W. and Greenberg, H. Extended limit design theorems for continuous media. *Quarterly of Applied Mathematics* **9**, 381–389 (1952).

[11] Anderheggen, E. and Knöpfel, H. Finite element limit analysis using linear programming. *International Journal of Solids and Structures* **8**, 1413–1431 (1972).

[12] Damkilde, L., Olsen, J. and Poulsen, P. N. A program for limit state analysis of plane, reinforced concrete plates by the stringer method. *Bygningsstatiske Meddelelser* **65** (1994).

[13] Poulsen, P. N. and Damkilde, L. Limit state analysis of reinforced concrete plates subjected to in-plane forces. *International Journal of Solids and Structures* **37**, 6011–6029 (2000).

[14] Sloan, S. W. Lower bound limit analysis using finite elements and linear programming. *International Journal for Numerical and Analytical Methods in Geomechanics* **12**, 61–77 (1988).

[15] Larsen, K. P. *Numerical Limit Analysis of Reinforced Concrete Structures.* Ph.D. thesis, Technical University of Denmark (2010).

[16] Herfelt, M. A., Poulsen, P. N., Hoang, L. C. and Jensen, J. F. Numerical rigid plastic modelling of shear capacity of keyed joints. In *Proceedings of the fib Symposium Copenhagen 2015* (2015).

[17] Boyd, S. P. and Vandenberghe, L. *Convex Optimization* (Cambridge University Press, 2004).